Effect of Polarity Reversal on the Enhanced Electrokinetic Remediation of 2,4-D-polluted Soils: A Numerical Study

López Vizcaíno, R.[a], Yustres, A.[a,*], Sáez, C.[b], Cañizares, P.[b], Rodrigo, M.A.[b], Navarro, V.[a]

[a]Geoenvironmental Group, Civil Engineering School, University of Castilla-La Mancha, Avda. Camilo José Cela s/n, 13071 Ciudad Real, Spain

[b]Department of Chemical Engineering, Faculty of Chemical Sciences & Technologies, University of Castilla-La Mancha, Campus Universitario s/n, 13071 Ciudad Real, Spain

*** Corresponding author:** angel.yustres@uclm.es, Civil Engineering School, University of Castilla-La Mancha, Avda. Camilo José Cela s/n, 13071 Ciudad Real, Spain

ABSTRACT

This article presents a numerical study of the transport phenomena involved in the electrokinetic remediation of soils polluted with polar pesticides. 2,4-Dichlorophenoxyacetic acid is used as a representative of this pesticide type. A one-dimensional configuration with two facing electrodes placed in electrolyte compartments and a cathodic overflow pollutant extraction system has been used for that purpose. The conventional electrokinetic remediation process is evaluated by keeping the electrode polarity constant, and to obtain acceptable yields, it is necessary to extend the treatment for more than 250 days. The application of periodic polarity reversals is proposed to improve these results. This strategy maximises the pesticide concentration in the cathodic compartment, thus maximising the pollutant extraction rate. The results show that by applying polarity reversals over 6-hour periods, it is possible to accelerate the treatment, thus improving its overall efficiency up to 94.5% compared with the treatment using a constant electrode polarity.

KEYWORDS

Electrokinetic soil remediation, Multiphysics simulation, Polarity Reversal, pesticide, M4EKR

1. INTRODUCTION

Electrokinetic remediation (EKR) is a competitive technology for treating polluted soils with low hydraulic conductivity. The objective of EKR is the mobilisation of pollutants towards controlled extraction points using a series of electrokinetic transport phenomena (the transport of fluids by electroosmosis, of ionic species by electromigration and of charged particles by electrophoresis) and thermal and hydraulic phenomena that occur in the soil when applying an electric potential gradient [1-4]. The range of physicochemical phenomena involved in this process broadens the EKR application field. This technology has been used to treat soils polluted with heavy metals [5-8], polycyclic aromatic hydrocarbons (PAH) [9, 10] and pesticides [11, 12], leading to favourable results.

Along with the electrokinetic transport phenomena, different electrochemical reactions can occur on the surface of electrodes. The most important reaction, regardless of the electrolyte composition, is water electrolysis. The oxidation of the water produced on the anodic surface generates protons (H^+), consequently reducing the pH. In exchange, hydroxyl ions (OH^-) are generated on the cathodic surface by the reduction reaction of water, producing a significant pH increase in the nearby soil. Both H^+ and OH^- are ionic species that move through the soil primarily by electromigration, producing two pH fronts, with an acidic front towards the cathode and a basic front towards the anode. The velocity of these fronts is primarily determined by the electromigration process of the ions involved and, to a lesser extent, by the advective/diffusive processes and the soil buffering capacity [13-17].

From an operational perspective, in addition to the magnitude, it is desirable to control the direction towards which the species are moved. This control is enabled by changing the sign of the electric gradient by reversing the electrode polarity. This operational strategy offers an important advantage since it facilitates the control of the direction of

pollutant movement, and it does not involve any additional treatment cost. This technique has been used to improve EKR processes in soils polluted with organic solvents [18, 19], petroleum-derived fuels [20, 21], PAHs [22, 23] and heavy metals [24]. However, its application in relation to the decontamination of soils with pesticides has only been studied in a few works [25, 26]. In recent years, great efforts have been made in the remediation of soils polluted with pesticides, focusing on the study of EKR processes applied to the removal of the polar pesticide 2,4-dichlorophenoxyacetic acid (2,4-D) via pollutant extraction by cathodic well overflow [27-29]. The work performed for that purpose allowed for the development of the M4EKR module (Multiphysics for EKR) [30], a multiphysics model developed by the authors and implemented in COMSOL Multiphysics [31]. M4EKR enables characterising and describing the processes that occur during the EKR of natural soil. Therefore, it is a useful tool for performing a numerical inspection that allows researchers to analyse the EKR treatment of soils polluted with 2,4-D as well as to evaluate the potential improvements afforded by the application of periodic polarity reversals. This application is the primary objective of the present work. In addition, owing to the capabilities of M4EKR, an operational strategy that increases treatment efficiency is analysed. To that end, an analysis of the mass flows associated with each transport process is performed, thus improving the overall understanding of each phenomenon. Although the theoretical direction of the mass flows associated with the different physical phenomena is widely known, the resulting total mass flow is not known a priori in all cases and for all species.

2. CONCEPTUAL AND NUMERICAL MODEL

The M4EKR module [30], which was used in this work, is a reactive transport model for partially saturated soils. For simplicity, the M4EKR version used in the present study does not include gas transport, and it does not consider the deformability of the soil. In

addition, it is assumed that the processes occur under isothermal conditions (298.15 K). Furthermore, the phenomena potentially involved in the mineralization of the pesticide, primarily microbial-mediated degradation and photodegradation, are not considered. In practice, this assumption would be true only in a completely sterile and non-irradiated soil. In addition, the adsorption onto the soil is also disregarded. Because of these simplifications, the model does not represent a real EKR process for soil contaminated with 2,4-D. However, the perfect modelization is not the objective of this work, but the objective is to contribute to a better understanding of the role of each flux during one of these remediation processes. Below is the mathematical formulation scheme, and greater detail can be found in López-Vizcaíno et al. [30].

2.1. Water mass balance

The equation used for the water mass balance is given by the expression:

$$\frac{\partial m_w}{\partial t} + \nabla \cdot \mathbf{l}_w = 0 \qquad [1]$$

where $\nabla\cdot$ is the divergence operator, $\mathbf{l}_w$ is the mass flow of water (kg m^{-2} s^{-1}) and m_w is the mass of water per unit total volume (kg m^{-3}). The van Genuchten retention curve model [32] is used to calculate m_w, and given that a non-deformable medium is assumed, the soil porosity is considered constant [30]. The water mass flux ($\mathbf{l}_w$) is given by the expression:

$$\mathbf{l}_w = \mathbf{l}_w^h + \mathbf{l}_w^{eo} = \rho_w \cdot \left(\mathbf{q}_w^h + \mathbf{q}_w^{eo}\right) \qquad [2]$$

where $\mathbf{l}_w^h$ is the hydraulic mass flux, $\mathbf{l}_w^{eo}$ is the electroosmotic flux, and $\mathbf{q}_w^h$ and $\mathbf{q}_w^{eo}$ are the associated volumetric fluxes (m s^{-1}), calculated using Darcy´s law and the semi-empirical Helmholtz-Smoluchowski formulation [33].

2.2. Reactive transport

The general geochemical system simulated in the M4EKR module considers a total of *J* components capable of generating a total of *N* chemical species during their combination. Therefore, to identify the chemical composition of the system, the total amounts of each component should be known through their corresponding mass balance equations, which have the following general form:

$$\frac{\partial m_j}{\partial t} + \nabla \cdot \mathbf{l}_j = R_j \qquad [3]$$

where m_j is the total mass of component *j* per unit total volume (mol m^{-3}), $\mathbf{l}_j$ is the total molar flux of component *j* (mol m^{-2} s^{-1}), and R_j is the rate of production or consumption of component *j* (mol m^{-3} s^{-1}). However, it is not necessary to solve *J* partial differential equations but rather to find the total of *J-2*, as the total mass of a component of the system can be determined by fulfilling the electroneutrality condition, and the mass balance of the water species is solved by equation 1.

The total molar flux of component *j* is calculated as follows:

$$\mathbf{l}_j = \mathbf{l}_j^h + \mathbf{l}_j^{eo} + \mathbf{l}_j^{em} + \mathbf{l}_j^{dif} \qquad [4]$$

where $\mathbf{l}_j^h$, $\mathbf{l}_j^{eo}$ and $\mathbf{l}_j^{em}$ are the advective flows generated by the hydraulic flow, the electroosmotic flow and the electromigration of ions, respectively, and $\mathbf{l}_j^{dif}$ is the Fickian diffusive-dispersive flow.

The chemical speciation problem is solved using a classical stoichiometric approach by solving a system of mass-balance and mass-action equations [34]. The mathematical formulation of this approach has been widely described in the literature [35, 36] and has been applied in M4EKR [30].

2.4. Electric charge balance

The balance equation of the total electric charge, with electroneutrality throughout the system and assuming that no charge accumulation capacity is present, is given by the following expression:

$$\nabla \cdot \mathbf{i} = 0 \qquad [5]$$

where **i** is the total current density (A m^{-2}), which is calculated by applying Ohm's law [30, 37] and using the empirical Rhoades formulation [38] for the apparent electrical conductivity of the soil and the formulation proposed by Appelo [39] for the electrical conductivity of pore water.

2.5. Mass balance in electrolyte wells

The electrolyte wells are necessary to the EKR processes for adding the washing fluid and for removing the collected pollutants. In the present study, two wells in which the electrodes are placed are considered, and they can alternately be either anodes or cathodes. To distinguish between them, they are called the LEC (Left Electrolyte Compartment) and the REC (Right Electrolyte Compartment).

In addition, since the geochemical model used here has a total of *N* species generated through the combination of *J* components [36] and it has been assumed that the electrolyte compartments behave as ideal continuous stirred tank reactors, *J-2* balance equations are used to determine the component mass evolution (the same as in the soil). Each electrolyte compartment has the following ordinary differential equation for the mass balance of each component:

$$\frac{\partial M_j^*}{\partial t} = \dot{M}_j^{in,*} - \dot{M}_j^{out,*} + R_j^* \qquad [6]$$

where the * superscript is equal to LEC or REC, depending on the affected well, R_j is the production or consumption flow of the component (mol s^{-1}) according to the electrochemical reactions, M_j is the total mass of component *j* as expressed in moles and $\dot{M}_j$ represents the input (superscript in) or output (superscript out) for the mass flows of component *j* (mol s^{-1}). The mathematical expressions used to determine these flows depend on whether the electrode located in the evaluated compartment acts as an anode or a cathode. These flows, as well as R_j and M_j, are defined in a previous study in which the complete formulation of the numerical model is described in detail [30]. It is interesting to note that the output of the pollutant from the system only occurs by overflow in the well where the cathode is located, and it moves towards the direction in which the electroosmotic water flow is moving.

2.6. Numerical implementation

The M4EKR model was completely implemented in the partial differential equation solver known as COMSOL Multiphysics [31]. This software is based on the application of the finite element method with Lagrange multipliers. The system of differential and algebraic equations to solve was fully defined by the authors. This approach is possible due to the versatility and adaptability of this type of program because of its multiphysics environment [40]. In addition, the automatic differentiation techniques [41] included in some programs, such as COMSOL Multiphysics, provide symbolic expressions for defining the iteration matrix [42], which improves the convergence behaviour of the model and allows the complexity of the problem to increase while the solution efficiency is maintained [43, 44]. One of the differentiating features of the code is that it includes the mass-balance and mass-action algebraic equations of the stoichiometric approach. This approach is the most common one in geochemical codes [36, 45, 46], some of which,

such as the PHREEQC program [35], are coupled to other modules to create reactive transport codes, which use common operator-splitting procedures [47-49]. However, none of these procedures is used for speciation in the M4EKR module, but the system of equations in the geochemical system is solved by COMSOL Multiphysics (Monolithic approach). In this way, a large number of state variables must be solved in a coupled manner at each time step and in all cases. Finally, for more clarity regarding the analysis, a one-dimensional configuration is used.

3. SIMULATION OF THE EKR PROCESS

3.1. Modelled configuration

3.1.1. Polluted soil

The EKR of a soil polluted with 2,4-D pesticide at an initial concentration of 20 mg $kg^{-1}_{dry\ soil}$ was studied. The analysed soil corresponds to the material from a quarry located in Toledo (central Spain). It is a low-plasticity clay (CL) according to the Unified Soil Classification System. Table 1 shows the mineralogical composition and textural parameters of the modelled soil. A natural density of 1.89 g cm^{-3} and a gravimetric water content of 32.8% [50] were set. After the material was analysed, the hydraulic parameters in Table 2 were obtained.

Table 1. Textural and mineralogical properties of the modelled soil.

Mineralogical Analysis	
Mineral	**Mass percentage (%)**
Quartz	7
Feldspar	15
Calcite	4
Kaolinite	26
Smectite	28
Illite	20
Textural Parameters	
Size fraction	**Mass percentage (%)**

Sand	26.9
Silt	68.2
Clay	4.9

Table 2. Soil hydraulic parameters**.**

Parameters	Description	Values	Units
α_{VG}	Parameter of the Van Genuchten retention curve	0.0147	kPa^{-1}
n_{VG}	Parameter of the Van Genuchten retention curve	1.2593	-
m_{VG}	Parameter of the Van Genuchten retention curve	0.2059	-
ϕ	Porosity	0.4681	-
K_{sat}^{h}	Saturated hydraulic permeability	2.03×10^{-10}	$m\ s^{-1}$
K_{sat}^{eo}	Saturated electroosmotic permeability	2.4×10^{-9}	$m^2\ V^{-1}\ s^{-1}$
ρ_s	Soil particle density	2681.5	$kg\ m^{-3}$
δ_i^L	Longitudinal dispersivity of species *i*	0.01	m
τ	Tortuosity	1.00	-

3.1.2. Pore water

To simplify the interpretation of the results, synthetic soil pore water is used in which a NaCl solution and the pesticide provide all the ionic strength. Thus, the geochemical model proposed for the soil pore water is composed of 5 components and 9 species. Table 3 shows a complete list along with the equilibrium reactions involved, their respective thermodynamic constants [51] and their physicochemical properties. The diffusion coefficients (D^o) not found in the literature are calculated using the Pikal expression [52]. The activity coefficients are determined using the WATEQ Debye-Hückel model [35].

Table 3. Thermodynamic properties of the modelled geochemical systems.

Species	Reactions	logK^{eq} (25ºC)	Hard-core diameter/Å	D^o / m^2s^{-1}
Cl^-	Cl^-	0	3.6	2.03×10^{-9}
H_2O	H_2O	0	3.4	5.27×10^{-9}
H^+	H^+	0	4.1	9.31×10^{-9}
Na^+	Na^+	0	4.1	1.33×10^{-9}
2,4-D^-	2,4-D^-	0	3.4	6.50×10^{-10}
OH^-	$H_2O \leftrightarrow OH^- + H^+$	-14	3.6	5.27×10^{-9}
NaOH	$Na^+ + H_2O \leftrightarrow NaOH + H^+$	-14.75	3.4	$1.89\times10^{-10*}$
NaCl	$Na^+ + Cl^- \leftrightarrow NaCl$	-0.5	3.4	$1.89\times10^{-10*}$
2,4-D	2,4-D^- + $H^+ \leftrightarrow$ 2,4-D	2.73	3.4	6.50×10^{-10}

* Obtained by using Pikal's model [52]

3.1.3. Modelled experimental setup

The behaviour of a laboratory-scale EKR reactor is simulated to reduce the computing times. The EKR reactor consists of two electrolyte compartments (15 × 3 × 3 cm) and a central compartment to contain the soil that is treated (15 × 15 × 3 cm). The electrodes are located inside the electrolyte compartments and have an electrochemically active surface of 45 cm^2, coinciding with the soil/electrolyte compartment interface. The electrolyte volume is kept constant during the entire simulation process at a value of 135 cm^3. To that end, a net addition of electrolyte to the compartments that act as anodes is used to maintain a constant level as well as overflow extraction in the cathodes. Figure 1

shows a schematic of the dimensions of the modelled system as well as the arrangement of the electrolyte compartments.

3.1.4. Initial conditions

Table 4 shows the initial conditions applied in the cases studied here. The electrolyte composition corresponds to a 9.53×10^{-4} molal NaCl solution and has a neutral pH (7). The soil pore water is composed of water with the same composition and an additional amount of 2,4-D corresponding to the pollution value (20 mg $kg^{-1}_{dry\ soil}$) with a total ionic strength of 9.52×10^{-4} molal.

3.1.5. Boundary conditions

The imposed boundary conditions are summarised in Figure 1. An electric gradient of 1 V cm^{-1} is applied in all cases, although in the polarity reversal simulations, its direction varies over time. For the water mass balance, it is assumed that P_L remains constant and equal to the atmospheric pressure (100 kPa), and for the balance of the chemical components, the concentration at the boundaries is assumed to be equal to the concentration in the electrolyte compartments.

Table 4. Initial conditions.

Total Concentration			Pore Water Chemical Speciation		Hydraulic		Electrical	
Molal	**Pore water**	**Electrolyte**	**Molal**		**kPa**		**V**	
C_{H^+}	1.65×10^{-8}	-3.06×10^{-11}	a_{H^+}	1.00×10^{-7}	P_L	100	E	1
C_{Na^+}	9.53×10^{-4}	9.53×10^{-4}	a_{Na^+}	9.20×10^{-4}				
$C_{2,4D_{anion}}$	3.19×10^{-4}	0	$a_{2,4D_{anion}}$	3.08×10^{-4}				
			a_{H_2O}	9.99×10^{-1}				
			c_{Cl^-}	6.33×10^{-4}				
			I	9.52×10^{-4}				

3.2. EKR simulation: Constant polarity study

As a reference, an EKR test was simulated in which a selected electric potential gradient was applied while keeping the electrode polarity constant. In this case, the LEC acts as an anodic compartment and the REC acts as a cathodic compartment.

Figure 2 shows the spatial distribution of the pH and the concentrations of the two pesticide species present.

The evolution of the pH follows the characteristic tendency of EKR processes, with a very marked front that moves slowly. The acid front generated in the LEC advances more rapidly than the basic front because in the simulated case, no reaction involving a pH buffering effect is considered. Therefore, the difference observed in the transport between H^+ and OH^- is primarily given by the different diffusion coefficients (and therefore the electromigration) of both species (see Table 3). The acid front reaches the cathodic well after 3.75 days of simulation. From this point on, the pH of the soil remains constant, with values close to 2 during the entire test, presenting a profile such as the one shown in Figure 2A (1 month).

The system pH strongly influences the chemical speciation [16, 53]. Fig. 2B and 2C show the spatial distribution of the concentration for both species of 2,4-D considered in the simulation, the acid species (2,4-D_{acid}) and the anionic species (2,4-D_{anion}) generated through the dissociation reaction of the acid species. Initially, when the system pH is neutral, the pesticide is completely dissociated ($c_{2,4D_{anion}}$ = 3.19×10^{-4} molal; $c_{2,4D_{acid}}$ = 0 molal). After 1 h of testing, the pH front has moved 0.09 m, and a significant pH gradient is produced between the electrolyte compartments (pH 3 in the anolyte and pH 11 in the catholyte). At this time, a decrease in $c_{2,4D_{anion}}$ is observed, which is more significant in the

soil regions close to the electrolyte compartments. By contrast, in the rest of the domain, the decrease in $c_{2,4D_{anion}}$ is moderate, and it is primarily related to the generation of 2,4-D_{acid} species in the soil regions between the anolyte and the pH front (acid region). As the pH front moves towards the cathodic well, the acidity of the soil is intensified. This intensification generates a substantial increase in $c_{2,4D_{acid}}$; consequently, there is less 2,4-D_{anion} in the domain. The 2,4-D_{acid} species move along with the pH front until reaching the catholyte (3.7 days/89 h). From this moment on, the spatial distribution of both species does not change shape, and there is only a change in magnitude, with a decreasing tendency over time. This trend indicates that the net transport of the pollutant occurs from the soil towards the electrolyte.

To improve our understanding of how the pesticide is transported, an analysis of the mass flows of the 2,4-D component is performed. The flows of each transport process are independently evaluated at the soil/electrolyte compartment interface (Figure 3).

Two different stages can be identified in the evolution of the flows: (i) before and (ii) after the pH front reaches the catholyte. Initially (stage (i)), the observed behaviour is similar at the LEC-soil (Fig. 3A) and REC-soil (Fig. 3B) interfaces. There is a net pesticide flow towards the electrolyte compartments with a significant diffusive component due to the substantial concentration gradient (as shown in Table 4, the electrolyte is initially free of 2,4-D). In addition, a mass flow is produced there by the electromigration process towards the LEC (anodic well) due to the negative charge of the 2,4-D_{anion} species. There is also an advective component (hydraulic and electroosmotic flow) moving from the LEC towards the REC during the entire test, which is greater in magnitude at the LEC-soil interface. This behaviour can be explained by considering the rapid desaturation presented by the soil in the regions near the anode and the consequent

296 increase in the hydraulic flow due to the associated suction gradient [30, 54, 55]. As the
297 test occurs, the pesticide concentrations in the electrolyte compartments and the soil
298 equalize, reducing the initial concentration gradient and the diffusive flow. This decrease
299 produces a reduction in the total pesticide flow from the soil towards the electrolyte
300 compartments.

301 When the pH front reaches the catholyte (REC), significant changes are observed in the
302 evolution of the mass flows. At this stage (ii), an increase in the diffusive flow is produced
303 at the REC-soil interface due to the increase of the pesticide concentration in this region
304 of the soil (see Fig. 2C). There is a very low total mass flow (10^{-10} $mol_{2,4\text{-}D}$ m^{-2} s^{-1}) towards
305 the electrolyte that is practically identical to the advective component, and it is also very
306 small. The flow by electromigration is on the same order of magnitude and in the opposite
307 direction from the diffusion one, as required to fulfil the Nernst-Planck equation. At the
308 LEC-soil interface, the advective component of the flow is higher than the diffusive and
309 electromigration ones, generating a change in the net flow direction (114 h), which
310 changes from negative (towards the electrolyte) to positive (towards the soil).

311 The time evolution of the pesticide species concentration (Fig. 4) is consistent with the
312 evolution of the mass flow for the 2,4-D component described above. In Fig. 4A (anodic
313 compartment, LEC), an increase in the pesticide concentration is initially observed,
314 primarily for the acid species, until reaching 114 h of testing. At this moment, the
315 pesticide concentration presents a progressive decrease in accordance with the observed
316 change in direction of the net flow. However, in the cathodic compartment (REC), the
317 accumulation of observed pesticides is not particularly significant (Fig. 4B) because the
318 mass flows in that region are of a lower magnitude (Fig. 3) and primarily because it is in
319 this compartment where a net mass output is produced by overflow extraction ($M_j^{out,\,REC}$,
320 Fig. 1).

This behaviour translates into an efficiency loss in the EKR process because all the pesticides previously removed from the soil and the accumulated pesticides in the anolyte pollute the soil once again. At that time, they are transported towards the catholyte and are extracted from this compartment. This process is very slow, and 245 days of treatment are required to remove 90% of the pesticide from the simulated system. To improve the efficiency of the EKR process, it is necessary to reduce the treatment time by maximising the extraction rate of the pesticide mass ($M_j^{out, REC}$, Fig.1). The extraction rate, $M_j^{out, REC}$, is proportional to the pesticide concentration in the cathodic compartment. Considering the evolution of the pesticide concentration in the electrolyte compartments (Fig. 4), the application of periodic polarity reversals is proposed to transform the anodic compartment into the cathodic compartment (extraction point) at the moment when the maximum pesticide concentration is reached; in this case, the time to reach this maximum is 114 h (see Fig. 4A).

3.3. EKR simulation: Polarity reversal study

An EKR test is simulated by applying an electric potential gradient of 1 V cm^{-1} with polarity reversals for 114-h periods. Initially, the LEC acts as an anodic compartment and the REC acts as a cathodic compartment.

Figures 5A and B show the evolution over time of the pesticide concentration in the electrolyte compartments. The observed behaviour is similar in both cases. When the compartment acts as an anode, a rapid increase in the concentration occurs until reaching a maximum value, the moment at which the polarity is inverted. At this instant, a sudden drop in the concentration occurs. This decrease corresponds with the extraction rate peaks shown in Fig. 5C. In this figure, it is also possible to observe that the global pesticide extraction rate is significantly higher in the polarity reversal test, which translates into a

346 faster global pesticide removal rate, which can be confirmed in the curves of the mass of
347 2,4-D extracted from the system (Fig. 5C, dotted lines).

348 With this operating strategy, pesticide accumulation in the anolyte and the returns to the
349 soil are avoided, thus accelerating the pollutant extraction process (94 days of treatment
350 to remove 90% of the pesticide). Therefore, this approach provides a more efficient global
351 pesticide removal than that obtained in the test with constant polarity.

352 The process improvement obtained by the change in polarity is confirmed. However, if
353 the evolution of the pesticide concentration in the cathodic compartments is analysed in
354 detail and in parallel to the extraction rate, it is clear that there is an important period in
355 each interval within which the concentration and the extraction rate decrease to values
356 similar to those obtained in the constant polarity test. It seems reasonable to expect that
357 if these periods are reduced, then the global efficiency of the EKR process can be
358 improved. Reducing the time of the polarity reversals is proposed to test this hypothesis.
359 For that purpose, three tests are simulated with polarity reversals of 24, 12 and 6 h.

360 Fig. 6 shows the yield evolution of the evaluated EKR processes, with the yield
361 understood as the percentage of the total removal of 2,4-D from the system.

362 The treatment time required to reach a determined removal yield decreases significantly
363 in all the cases in which the polarity reversal is applied. If the cases in which this strategy
364 is used are analysed, then the reduction of the time intervals at which the polarity of the
365 electrodes is inverted can be observed to produce an improvement in the given removal
366 yield. To quantify this improvement, Fig. 6B shows that the time used to reach a 2,4-D
367 removal yield of 90% decreases significantly, from 254 h in the treatment with constant
368 polarity to 14 h when the polarity reversal is applied over 6-h periods. This result reflects

a 94.5% reduction in the treatment time, which consequently leads to a minimisation in the energy consumption required to reach the established decontamination levels.

4. CONCLUSIONS

In this study, a numerical model is presented for treating soils polluted with 2,4-D pesticide using an electrokinetic remediation process consisting of pollutant extraction through the overflow of the cathodic compartment. First, the pesticide transport during an EKR process is evaluated by applying an electric gradient of 1 V cm^{-1}, maintaining a constant electrode polarity. In this study, the maximum pesticide concentration within the cathodic compartment is very low; therefore, the removal of the pesticide from the system is a slow process (254 days). However, the pesticide concentrates rapidly and at a higher magnitude in the anodic compartment. To account for this behaviour, the use of periodic polarity reversals is proposed to improve the treatment efficiency. This operational strategy enables converting the anodic compartment, where the pesticide is primarily concentrated, into a cathodic compartment from which the pollution extraction occurs. This process occurs alternatively in the opposite electrolyte compartments. Using this strategy, the pesticide concentration is maximised in both electrolyte compartments; therefore, the pollutant extraction has a reduced treatment time of 94.5% when polarity reversal is applied over 6-h periods compared with the case in which the extraction is simulated under constant polarity.

ACKNOWLEDGEMENTS

The financial support from the Spanish Ministry of Economy, Industry and Competitiveness and the European Union through projects [CTM2013-45612-R] and [CTM2016-76197-R (AEI/FEDER, UE)] is gratefully acknowledged.

REFERENCES

[1] Y.B. Acar, Principles of electrokinetic remediation, Environment Science Technology, 27 (1993) 2638-2647.

[2] J. Virkutyte, M. Sillanpaa, P. Latostenmaa, Electrokinetic soil remediation - critical overview, Sci. Total Environ., 289 (2002) 97-121.

[3] Y.B. Acar, R.J. Gale, A.N. Alshawabkeh, R.E. Marks, S. Puppala, M. Bricka, R. Parker, Electrokinetic remediation: Basics and technology status, J. Hazard. Mater., 40 (1995) 117-137.

[4] K.R. Reddy, C. Cameselle, Electrochemical Remediation Technologies for Polluted Soils, Sediments and Groundwater, John Wiley and Sons2009.

[5] L.M. Ottosen, H.K. Hansen, A.B. Ribeiro, A. Villumsen, Removal of Cu, Pb and Zn in an applied electric field in calcareous and non-calcareous soils, J. Hazard. Mater., 85 (2001) 291-299.

[6] M. Mascia, S. Palmas, A.M. Polcaro, A. Vacca, A. Muntoni, Experimental study and mathematical model on remediation of Cd spiked kaolinite by electrokinetics, Electrochimica Acta, 52 (2007) 3360-3365.

[7] C. Vereda-Alonso, C. Heras-Lois, C. Gomez-Lahoz, F. Garcia-Herruzo, J.M. Rodriguez-Maroto, Ammonia enhanced two-dimensional electrokinetic remediation of copper spiked kaolin, Electrochimica Acta, 52 (2007) 3366-3371.

[8] V. Ferri, S. Ferro, C.A. Martínez-Huitle, A. De Battisti, Electrokinetic extraction of surfactants and heavy metals from sewage sludge, Electrochimica Acta, 54 (2009) 2108-2118.

[9] M. Pazos, E. Rosales, T. Alcántara, J. Gómez, M.A. Sanromán, Decontamination of soils containing PAHs by electroremediation: A review, J. Hazard. Mater., 177 (2010) 1-11.

[10] J.N. Hahladakis, N. Lekkas, A. Smponias, E. Gidarakos, Sequential application of chelating agents and innovative surfactants for the enhanced electroremediation of real sediments from toxic metals and PAHs, Chemosphere, 105 (2014) 44-52.

[11] A.B. Ribeiro, J.M. Rodriguez-Maroto, E.P. Mateus, H. Gomes, Removal of organic contaminants from soils by an electrokinetic process: the case of atrazine. Experimental and modeling, Chemosphere, 59 (2005) 1229-1239.

[12] M.A. Rodrigo, N. Oturan, M.A. Oturan, Electrochemically assisted remediation of pesticides in soils and water: a review, Chemical reviews, 114 (2014) 8720-8745.

[13] J.M. Paz-Garcia, K. Baek, I.D. Alshawabkeh, A.N. Alshawabkeh, A generalized model for transport of contaminants in soil by electric fields, Journal of Environmental Science and Health - Part A Toxic/Hazardous Substances and Environmental Engineering, 47 (2012) 308-318.

[14] S.K. Puppala, A.N. Alshawabkeh, Y.B. Acar, R.J. Gale, M. Bricka, Enhanced electrokinetic remediation of high sorption capacity soil, J. Hazard. Mater., 55 (1997) 203-220.

[15] K.R. Reddy, U.S. Parupudi, S.N. Devulapalli, C.Y. Xu, Effects of soil composition on the removal of chromium by electrokinetics, J. Hazard. Mater., 55 (1997) 135-158.

[16] A.Z. Al-Hamdan, K.R. Reddy, Geochemical assessment of metal transport in glacial till during electrokinetic remediation, Environmental Monitoring and Assessment, 139 (2008) 137-149.

[17] A.Z. Al-Hamdan, K.R. Reddy, Transient behavior of heavy metals in soils during electrokinetic remediation, Chemosphere, 71 (2008) 860-871.

[18] Q. Luo, H. Wang, X. Zhang, X. Fan, Y. Qian, In situ bioelectrokinetic remediation of phenol-contaminated soil by use of an electrode matrix and a rotational operation mode, Chemosphere, 64 (2006) 415-422.

443 [19] A. Oonnittan, R.A. Shrestha, M. Sillanpaa, Removal of hexachlorobenzene from soil
444 by electrokinetically enhanced chemical oxidation, J. Hazard. Mater., 162 (2009) 989-
445 993.
446 [20] E. Mena, J. Villaseñor, M.A. Rodrigo, P. Cañizares, Electrokinetic remediation of
447 soil polluted with insoluble organics using biological permeable reactive barriers: Effect
448 of periodic polarity reversal and voltage gradient, Chem. Eng. J., 299 (2016) 30-36.
449 [21] T. Li, S. Guo, B. Wu, L. Zhang, Y. Gao, Effect of polarity-reversal and electrical
450 intensity on the oil removal from soil, Journal of Chemical Technology and
451 Biotechnology, 90 (2015) 441-448.
452 [22] T. Li, Y. Wang, S. Guo, X. Li, Y. Xu, Y. Wang, X. Li, Effect of polarity-reversal on
453 electrokinetic enhanced bioremediation of Pyrene contaminated soil, Electrochimica
454 Acta, 187 (2016) 567-575.
455 [23] K.R. Reddy, R.E. Saichek, Enhanced Electrokinetic Removal of Phenanthrene from
456 Clay Soil by Periodic Electric Potential Application, Journal of Environmental Science
457 and Health - Part A Toxic/Hazardous Substances and Environmental Engineering, 39
458 (2004) 1189-1212.
459 [24] M. Pazos, M.A. Sanromán, C. Cameselle, Improvement in electrokinetic remediation
460 of heavy metal spiked kaolin with the polarity exchange technique, Chemosphere, 62
461 (2006) 817-822.
462 [25] S. Barba, J. Villaseñor, M.A. Rodrigo, P. Cañizares, Effect of the polarity reversal
463 frequency in the electrokinetic-biological remediation of oxyfluorfen polluted soil,
464 Chemosphere, 177 (2017) 120-127.
465 [26] E. Vieira dos Santos, C. Sáez, P. Cañizares, C.A. Martínez-Huitle, M.A. Rodrigo,
466 Reversible electrokinetic adsorption barriers for the removal of atrazine and oxyfluorfen
467 from spiked soils, J. Hazard. Mater., 322 (2017) 413-420.

468 [27] C. Risco, R. López-Vizcaíno, C. Sáez, A. Yustres, P. Cañizares, V. Navarro, M.A.
469 Rodrigo, Remediation of soils polluted with 2,4-D by electrokinetic soil flushing with
470 facing rows of electrodes: A case study in a pilot plant, Chem. Eng. J., 285 (2016) 128-
471 136.
472 [28] C. Risco, S. Rodrigo, R. López-Vizcaíno, C. Sáez, P. Cañizares, V. Navarro, M.A.
473 Rodrigo, Electrokinetic flushing with surrounding electrode arrangements for the
474 remediation of soils that are polluted with 2,4-D: A case study in a pilot plant, Sci. Total
475 Environ., 545-546 (2016) 256-265.
476 [29] C. Risco, S. Rodrigo, R. López-Vizcaíno, A. Yustres, C. Sáez, P. Cañizares, V.
477 Navarro, M.A. Rodrigo, Electrochemically assisted fences for the electroremediation of
478 soils polluted with 2,4-D: A case study in a pilot plant, Separation and Purification
479 Technology, 156, Part 2 (2015) 234-241.
480 [30] R. López-Vizcaíno, A. Yustres, M.J. León, C. Saez, P. Cañizares, M.A. Rodrigo, V.
481 Navarro, Multiphysics Implementation of Electrokinetic Remediation Models for Natural
482 Soils and Porewaters, Electrochimica Acta, 225 (2017) 93-104.
483 [31] C. AB, COMSOL Multiphysics Reference Manual Version: COMSOL 5.1., (2015).
484 [32] M.T. van Genuchten, A Closed-form Equation for Predicting the Hydraulic
485 Conductivity of Unsaturated Soils1, Soil Science Society of America Journal, 44 (1980)
486 892-898.
487 [33] J.K. Mitchell, K. Soga, Fundamentals of soil behavior, John Wiley & Sons, Inc,
488 Hoboken, New Jersey, USA, 2005.
489 [34] A.M.M. Leal, M.J. Blunt, T.C. LaForce, Efficient chemical equilibrium calculations
490 for geochemical speciation and reactive transport modelling, Geochimica et
491 Cosmochimica Acta, 131 (2014) 301-322.

[35] D.L. Parkhurst, C.A.J. Appelo, User's guide to PHREEQ C (Version 2) – a computer program for speciation, batch-reaction, one-dimensional transport and inverse geochemical calculations, Water-Resources Investigations, Report 99–4259, Denver, Co, USA, (1999) 312.

[36] C.M. Bethke, Geochemical and Biogeochemical Reaction Modeling, Cambridge University Press2007.

[37] R.A. Jacobs, R.F. Probstein, Two-Dimensional Modeling of Electroremediation, AIChE Journal, 42 (1996) 1685-1696.

[38] J.D. Rhoades, N.A. Manteghi, P.J. Shouse, W.J. Alves, Soil Electrical Conductivity and Soil Salinity: New Formulations and Calibrations, Soil Science Society of America Journal, 53 (1989) 433-439.

[39] C.A.J. Appelo, Specific conductance: how to calculate, to use, and the pitfalls, 2010.

[40] D.E. Keyes, L.C. McInnes, C. Woodward, W. Gropp, E. Myra, M. Pernice, J. Bell, J. Brown, A. Clo, J. Connors, E. Constantinescu, D. Estep, K. Evans, C. Farhat, A. Hakim, G. Hammond, G. Hansen, J. Hill, T. Isaac, X. Jiao, K. Jordan, D. Kaushik, E. Kaxiras, A. Koniges, K. Lee, A. Lott, Q. Lu, J. Magerlein, R. Maxwell, M. McCourt, M. Mehl, R. Pawlowski, A.P. Randles, D. Reynolds, B. Rivière, U. Rüde, T. Scheibe, J. Shadid, B. Sheehan, M. Shephard, A. Siegel, B. Smith, X. Tang, C. Wilson, B. Wohlmuth, Multiphysics simulations: Challenges and opportunities, International Journal of High Performance Computing Applications, 27 (2013) 4-83.

[41] F. Palacios, J. Alonso, K. Duraisamy, M. Colonno, J. Hicken, A. Aranake, A. Campos, S. Copeland, T. Economon, A. Lonkar, T. Lukaczyk, T. Taylor, Stanford University Unstructured (SU2): An open-source integrated computational environment for multi-physics simulation and design, 51 st AIAA Aerospace Sciences Meeting including the New Horizons Forum and Aerospace Exposition, (2013).

517 [42] M.K. Gobbert, A. Churchill, G. Wang, T.I. Seidman, COMSOL Multiphysics for
518 efficient solution of a transient reaction-diffusion system with fast reaction, Y. Rao (Ed.)
519 COMSOL Conference 2009 Boston, USA, (2009).
520 [43] V. Navarro, L. Asensio, T. Yustres, X. Pintado, J. Alonso, An elastoplastic model of
521 bentonite free swelling, Engineering Geology, 181 (2014) 190-201.
522 [44] V. Navarro, L. Asensio, Á. Yustres, G. De la Morena, X. Pintado, Swelling and
523 mechanical erosion of MX-80 bentonite: Pinhole test simulation, Engineering Geology,
524 202 (2016) 99-113.
525 [45] J.W. Ball, D.K. Nordstrom, D.W. Zachmann, WATEQ4F - A personal computer
526 FORTRAN translation of the geochemical model WATEQ2 with revised database, US
527 Geol. Surv. Open-File Rep., 87 (1987).
528 [46] J.M. Paz-García, B. Johannesson, L.M. Ottosen, A.B. Ribeiro, J.M. Rodríguez-
529 Maroto, Simulation-based analysis of the differences in the removal rate of chlorides,
530 nitrates and sulfates by electrokinetic desalination treatments, Electrochimica Acta, 89
531 (2013) 436-444.
532 [47] J. Carrayrou, R. Mosé, P. Behra, Operator-splitting procedures for reactive transport
533 and comparison of mass balance errors, Journal of Contaminant Hydrology, 68 (2004)
534 239-268.
535 [48] D. Jacques, J. Šimůnek, D. Mallants, M.T. van Genuchten, Operator-splitting errors
536 in coupled reactive transport codes for transient variably saturated flow and contaminant
537 transport in layered soil profiles, Journal of Contaminant Hydrology, 88 (2006) 197-218.
538 [49] J.M. Paz-García, B. Johannesson, L.M. Ottosen, A.N. Alshawabkeh, A.B. Ribeiro,
539 J.M. Rodríguez-Maroto, Modeling of electrokinetic desalination of bricks,
540 Electrochimica Acta, 86 (2012) 213-222.

[50] R. López-Vizcaíno, V. Navarro, M.J. León, C. Risco, M.A. Rodrigo, C. Sáez, P. Cañizares, Scale-up on electrokinetic remediation: Engineering and technological parameters, J. Hazard. Mater., 315 (2016) 135-143.

[51] E. Giffaut, M. Grivé, P. Blanc, P. Vieillard, E. Colàs, H. Gailhanou, S. Gaboreau, N. Marty, B. Madé, L. Duro, Andra thermodynamic database for performance assessment: ThermoChimie, Applied Geochemistry, 49 (2014) 225-236.

[52] M.J. Pikal, Ion-pair formation and the theory of mutual diffusion in a binary electrolyte, The Journal of Physical Chemistry, 75 (1971) 663-675.

[53] A.Z. Al-Hamdan, K.R. Reddy, Electrokinetic remediation modeling incorporating geochemical effects, J. Geotech. Geoenviron. Eng., 134 (2008) 91-105.

[54] S. Wieczorek, H. Weigand, M. Schmid, C. Marb, Electrokinetic remediation of an electroplating site: Design and scale-up for an in-situ application in the unsaturated zone, Engineering Geology, 77 (2005) 203-215.

[55] J. Yuan, M.A. Hicks, Influence of gas generation in electro-osmosis consolidation, International Journal for Numerical and Analytical Methods in Geomechanics, 40 (2016) 1570-1593.

564 **FIGURES**

565

566

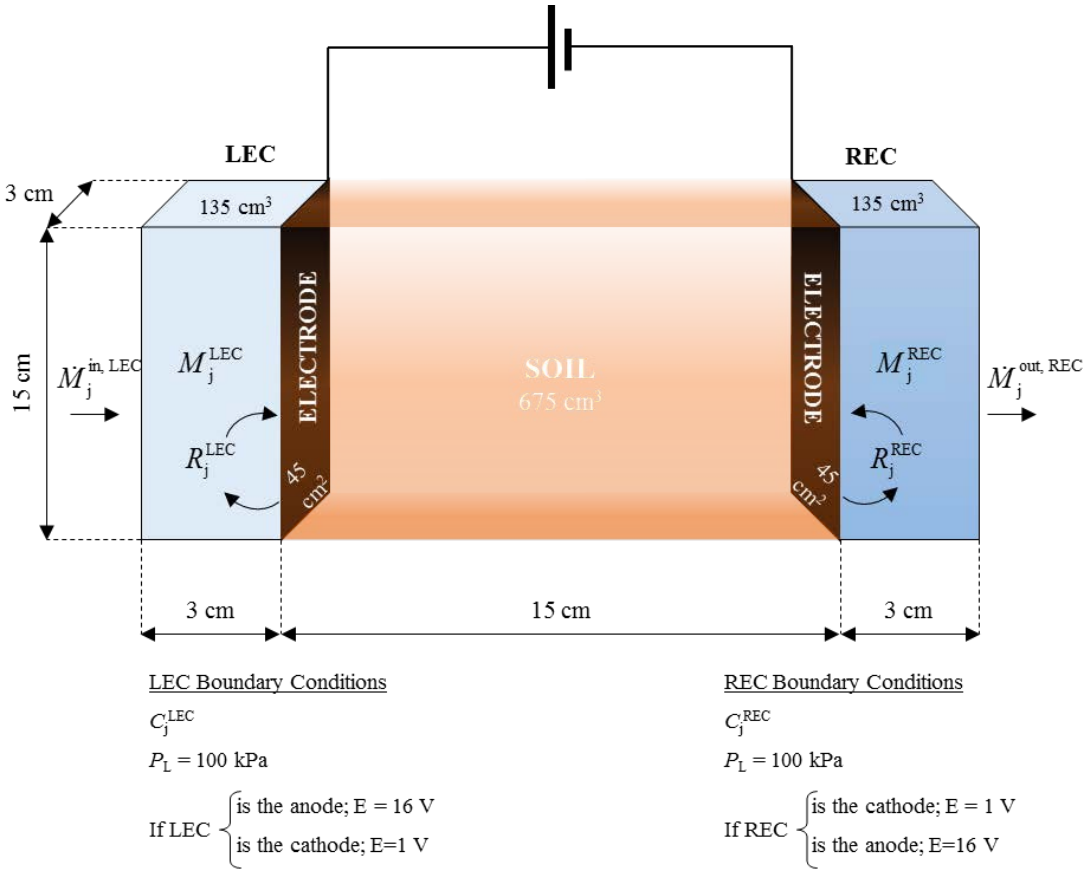

567

568 **Figure 1.** Conceptual model, dimensions of the one-dimensional domain and boundary

569 conditions of the modelled system.

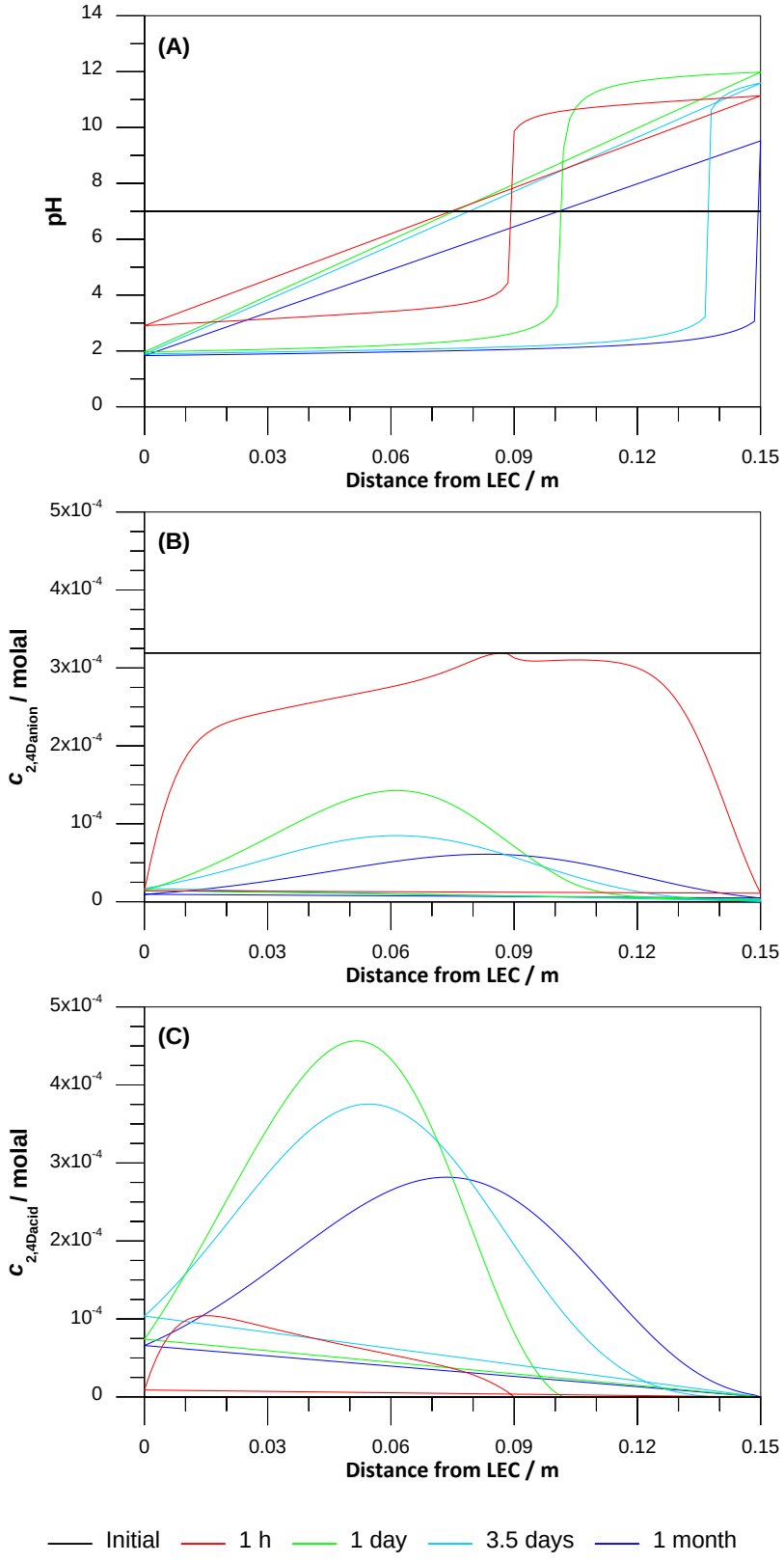

570

571 **Figure 2**. Spatial distribution in the EKR-constant polarity study at selected times for the

572 (A) pH; (B) total concentration of the 2,4-D_{anion} species; and (C) total concentrations of

573 the 2,4-D_{acid} species.

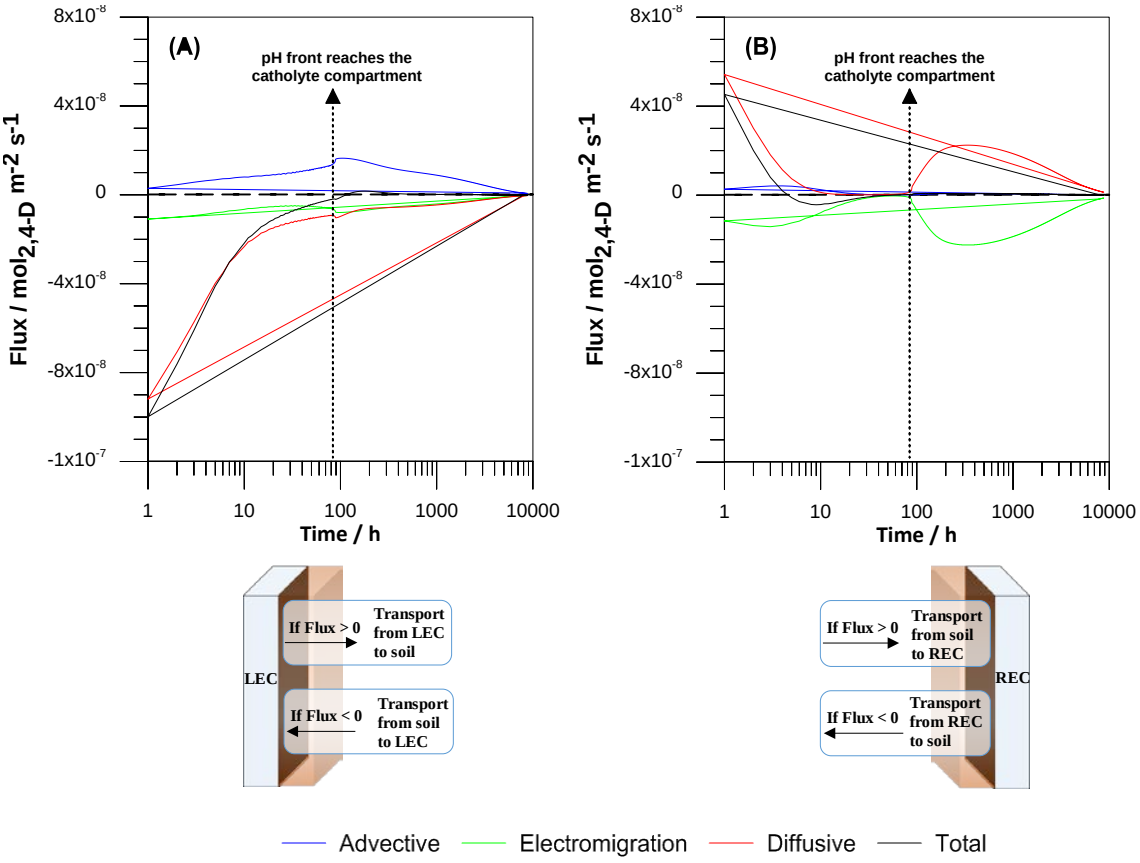

574

575 **Figure 3**. Temporal evolution of the total mass flows for the 2,4-D component.

576 Evaluation position: (A) LEC-Soil interface and (B) REC-Soil interface.

577

578

579

580

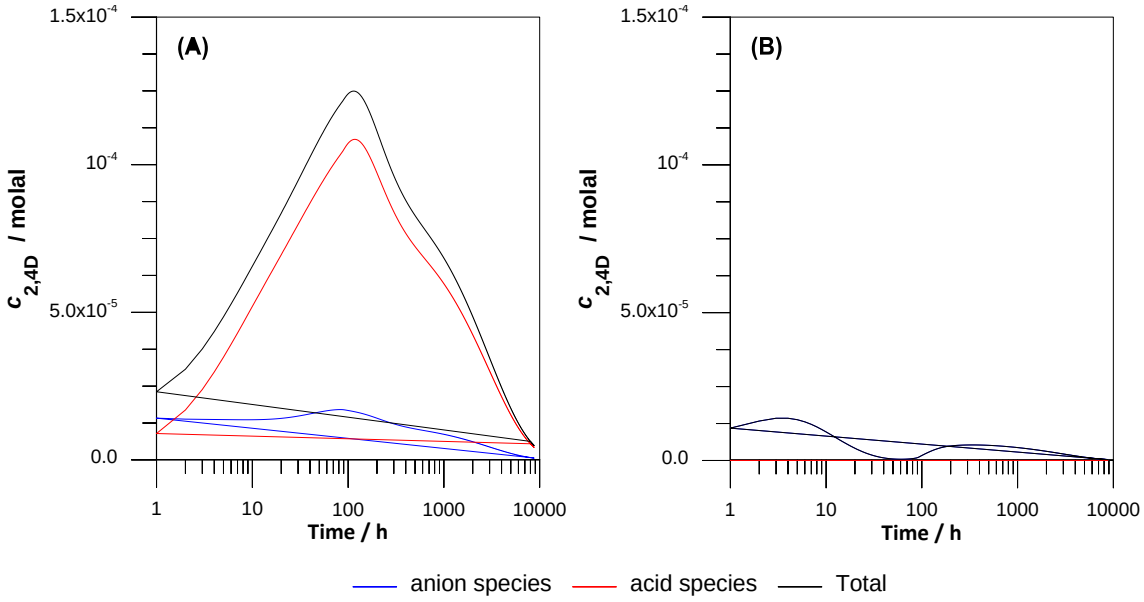

581

582 **Figure 4**. Temporal evolution of the 2,4-D species concentrations in the electrolyte

583 compartments: (A) LEC and (B) REC.

584

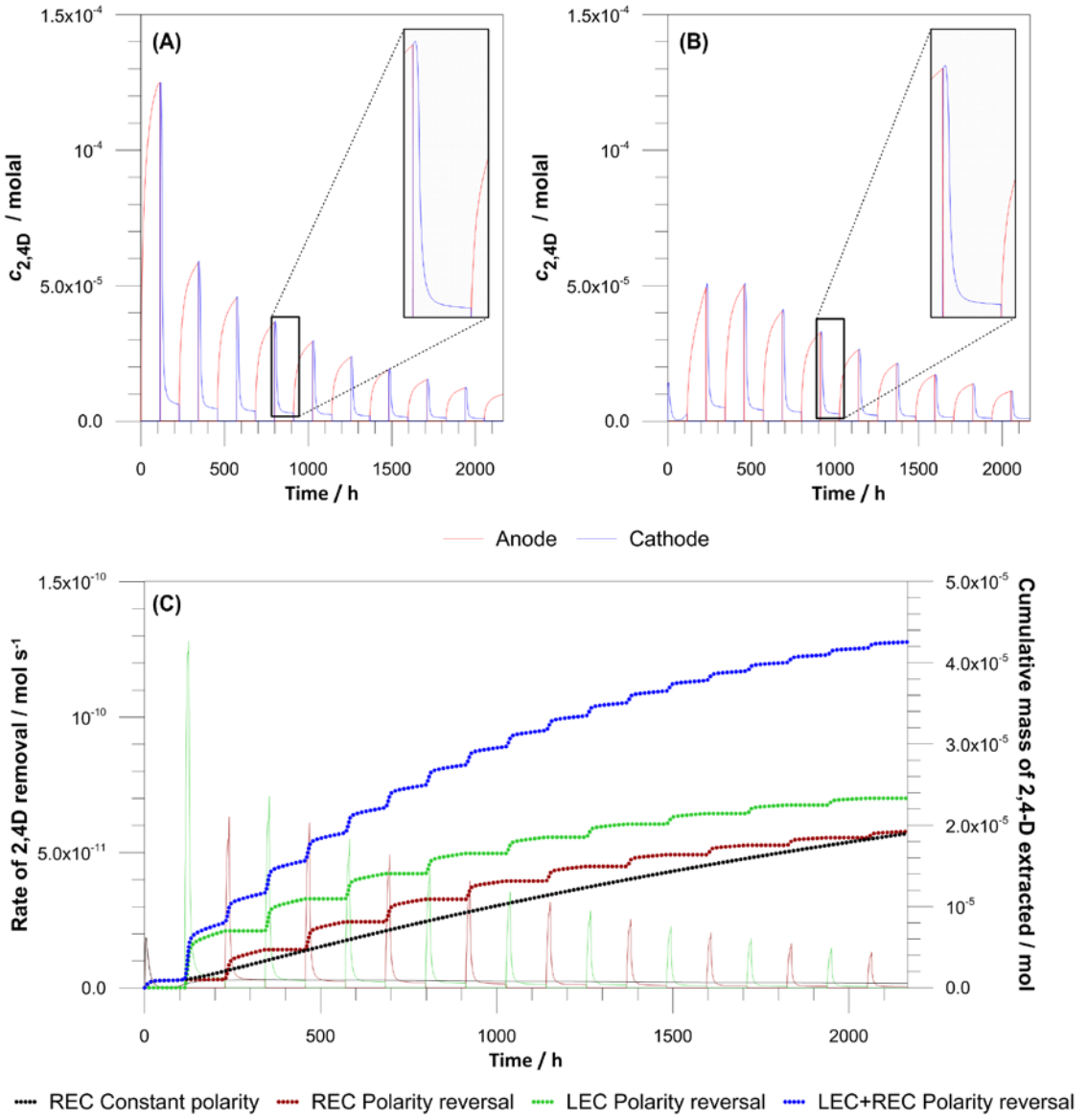

585

586 **Figure 5**. Temporal evolution of the 2,4-D component concentrations in the electrolyte
587 compartments for (A) LEC and (B) REC. Temporal evolution of the pesticide extraction
588 rate in the cathodic compartments (C, solid lines) and the mass of 2,4-D extracted (C,
589 dotted lines).

590

591

592

593

594

595

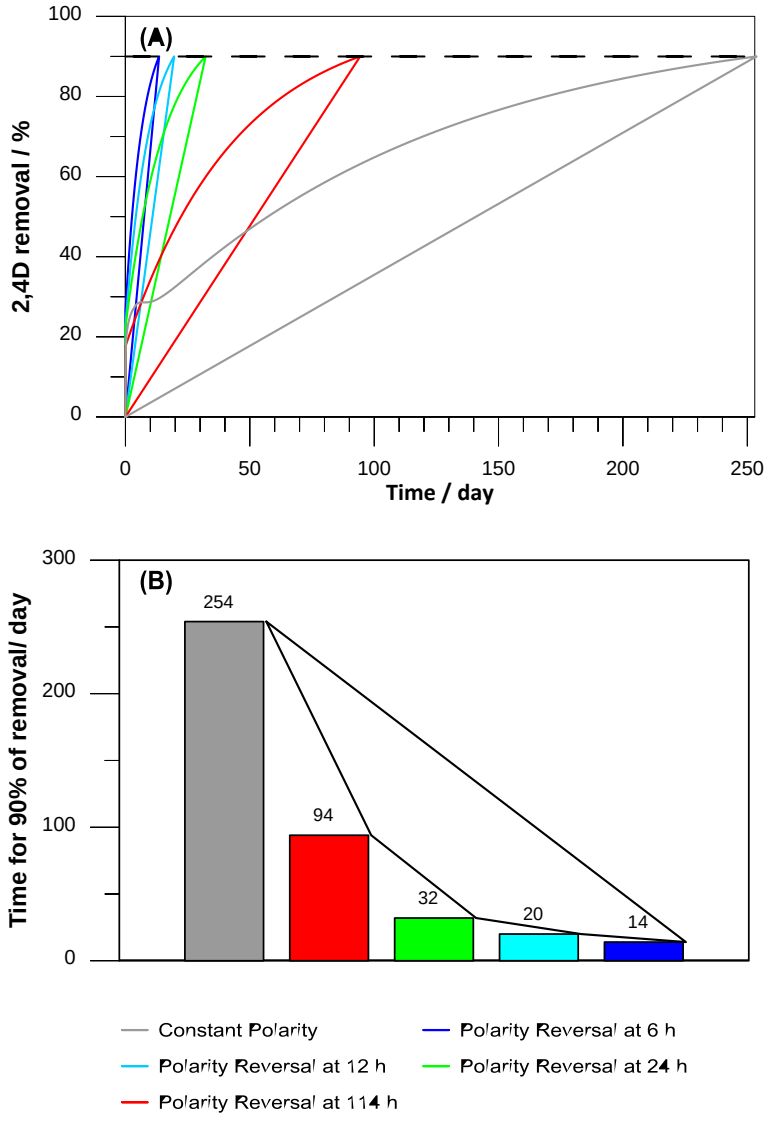

596

597 **Figure 6**. (A) Time evolution of the removal yield for the 2,4-D component with the
598 different evaluated strategies. (B) Time required to reach a 2,4-D removal yield of 90%
599 using the different evaluated strategies.

600

601

602